Supplementary Information (SI) for Energy Advances.

Effect of Zn/Mn in the supercapacitor behavior of high entropy FeCoNiCrZn/Mn alloy

Gobinda Chandra Mohanty[1], Chinmayee Chowde Gowda[1], Pooja Gakhad[2], M Sanjay[3], Abhishek Singh[2], Koushik Biswas[1,3*] and Chandra Sekhar Tiwary[1,3*]*

[1]School of Nano Science and Technology Indian Institute of Technology Kharagpur, West Bengal – 721302

[2]Materials Research Centre, Indian Institute of Science Bengaluru, Karnataka – 560012

[3]Department of Metallurgy and Materials Engineering Indian Institute of Technology Kharagpur, West Bengal – 721302

Corresponding authors: abhishek@iisc.ac.in (Abhishek Singh), k_biswas@metal.iitkgp.ac.in (Koushik Biswas) and chandra.tiwary@metal.iitkgp.ac.in (Chandra Sekhar Tiwary)

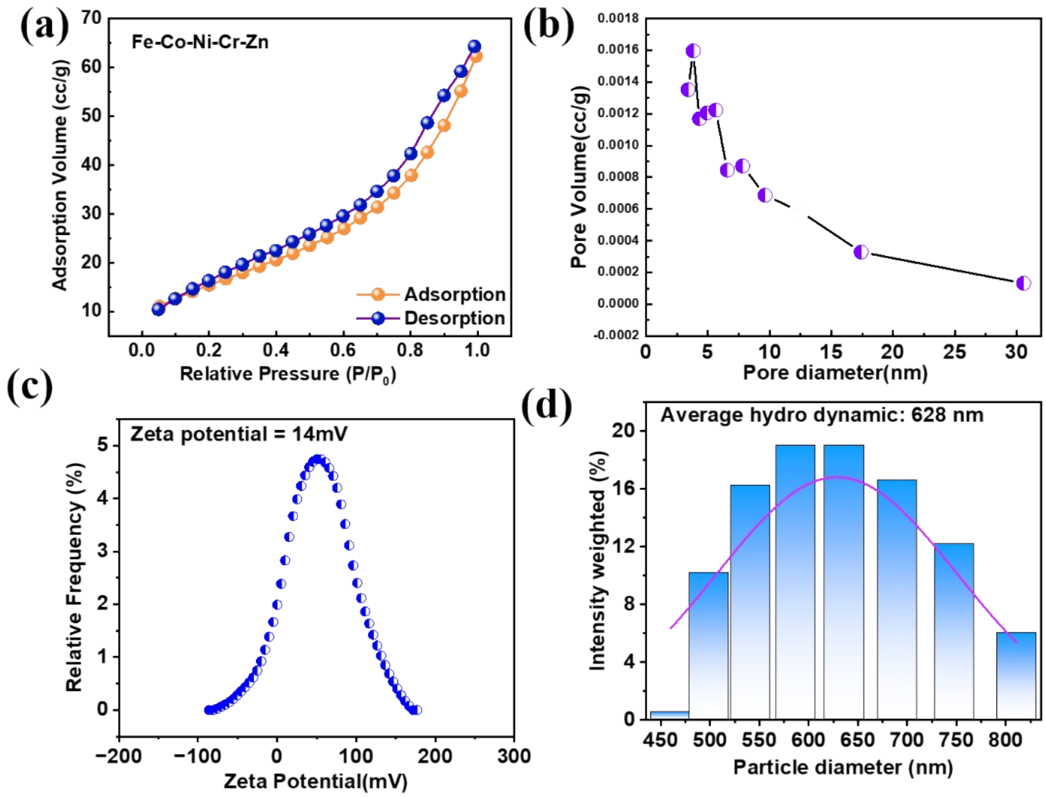

Figure S1: *(a) Adsorption desorption isotherm, (b) Pore diameter vs. pore volume, (c) Zeta potential and (d) Hydrodynamic particles size distribution of Fe-Co-Ni-Cr-Zn HEA powder.*

Electrochemical studies:

Electrochemical studies of nanostructured FeCoNiCrZn HEA electrodes were performed using BioLogic SP-200 (France) electrochemical work station. The working electrode was prepared by using this quinary FeCoNiCrZn HEA with 70 wt% of active material along with 20 wt% of activated carbon and 10wt% of PVDF. NMP (solvent) was added to the above mixture to create a homogeneous slurry after grinding in a mortar and pestle, then ultrasonicating the ink for 30 min. The slurry is then coated onto 1 cm^2 of battery grade graphite sheet (post-acetone wash) (size 1 x 2 cm^2, thickness 0.2 mm) and followed by drying at 60 °C overnight in a vacuum oven. Later, the HEA-coated graphite sheet, platinum wire and Ag/AgCl were used as working, counter and reference electrode, respectively for the three electrode measurement system. All electrochemical measurements were taken in the optimized concentration of aqueous KOH (3M) electrolyte. The supercapacitor study is explained with the assistance of cyclic voltammetry (CV), galvonostatic charge discharge (GCD), and electrochemical impedance spectroscopy (EIS).

The CV curves of FeCoNiCrZn show nonlinear curves for which the specific capacitance was calculated as[1,2]

$$C_s\left(F\,g^{-1}\right)=\frac{\int_{V_i}^{V_f} I(V)dV}{m\,\nu\left(V_f-V_i\right)} \qquad (S1)$$

Since FeCoNiCrZn HEA follows a non-triangular discharge process, the specific capacitance was calculated as [3],

$$C_s\left(F\,g^{-1}\right)=\frac{I\int Vdt}{m\left(V_f-V_i\right)^2} \qquad (S2)$$

$\int_{V_i}^{V_f} I(V)dV$, m, ν, $I\int Vdt$ and (V_f-V_i) are integral area under CV, mass loading, scan rate, integral area under discharge and potential window respectively.

An asymmetric supercapacitor (ASC) device is demonstrated with wide voltage window, high specific capacitance, and high specific energy with long cyclic stability. The device usually consists of two electrodes with balanced charge, weight, and corresponding stable voltage[4]. Further an electrochemical capacitor capacitance is expressed as specific capacitance (gravimetric F g^{-1}). The specific energy and specific power of the ASC device (which follows non-linear characteristics) are evaluated by **equation S3** and **equation S4**, respectively[5, 6]

$$E\left(Wh\,kg^{-1}\right)=\frac{I\int V\,dt}{m\ 3.6} \qquad (S3)$$

$$P\left(W\,kg^{-1}\right)=\frac{E}{\Delta t} \qquad (S4)$$

Where 'I' is current density, $\int V\,dt$ is the area under the discharge curve of the GCD plot, m is mass loading, E is energy density, and Δt is the charge time.

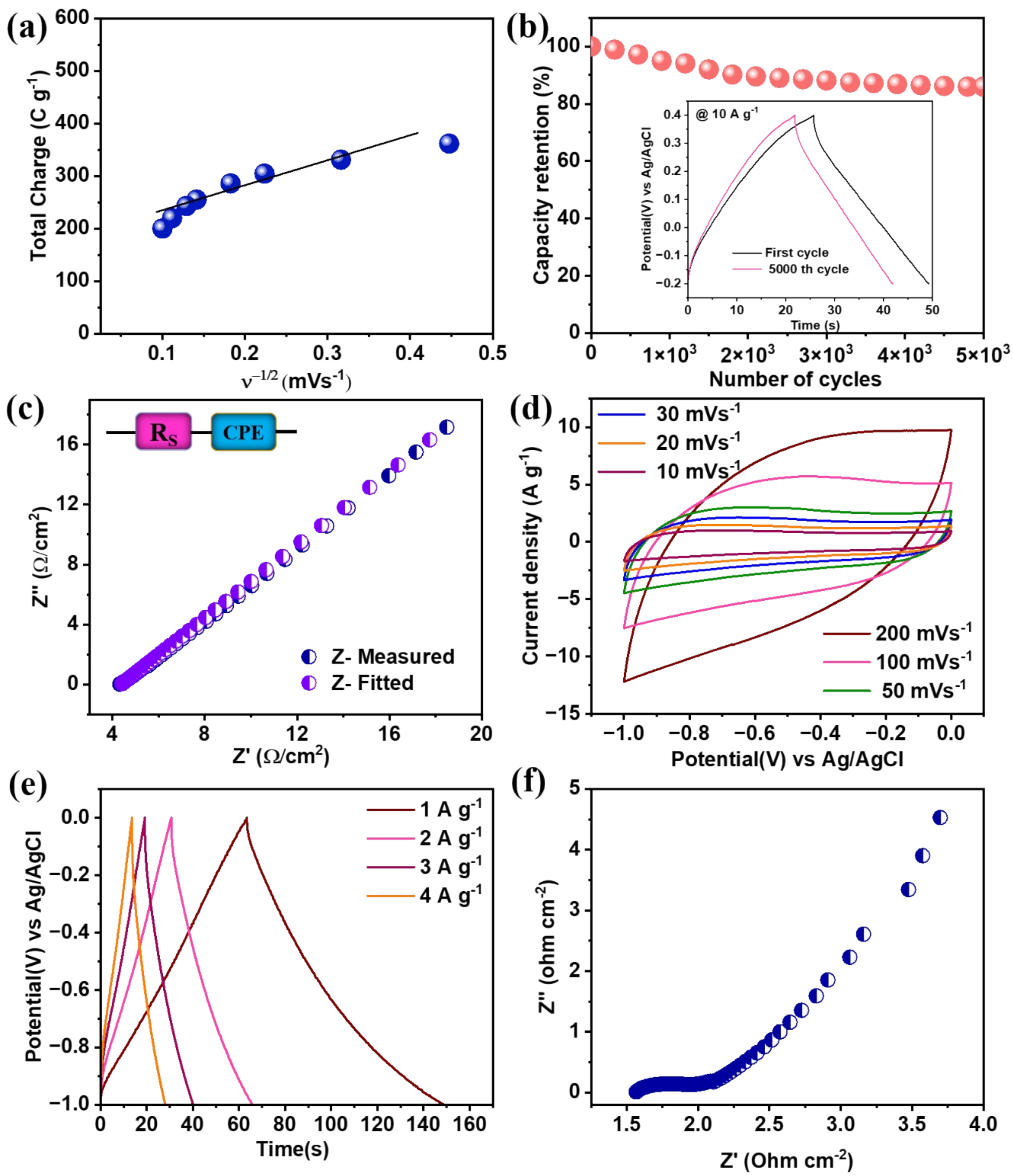

Figure S2*: (a) Total charge vs. scan rate for Fe-Co-Ni-Cr-Zn HEA electrode, (b) Cyclic stability at 10 A g^{-1} up to 5000 cycles, (c) EIS study for same electrode, (d, e, f) CV, GCD and EIS analysis of activated carbon as negative electrode.*

Device Characteristics:

For an electrochemical process, relaxation time constant (τ_0) defines the rate of electrochemical activities in terms of forming the boundary between resistive and capacitive activity. The **Figure S3(a)** shows that the bode plot defines energy storing capability for bode angle and frequency. The known phase angle for an ideal electrochemical double-layer capacitor is 90°, while for pseudo capacitive material, this value ranges between 45° to 90° [7]. Also, at 45° the capacitive and resistive components are equal[1]. Hence the value of τ is calculated from the bode plot is around 801 ms. This lower value of relaxation time facile moderate ion diffusion[8]. Similarly, frequency dependent imaginary and real capacitance parameter is shown in the **Figure S3(b)**. The value of C'' refers to power dissipation due to an uncomplimentary irreversible redox mechanism. The value of C' and C'' is calculated using the **equation S5 and S6**[9],

$$C' = \frac{-Z''}{2\pi f\ |Z|^2} \qquad (S5)$$

$$C'' = \frac{Z'}{2\pi f\ |Z|^2} \qquad (S6)$$

Also, the diffusion constant plays a major role in determining the electrode's electrochemical activity concerning the nature of electrolyte ions. The feasibility of K^+ ions into the multivalent HEA is clearly understood from the diffusion constant. The Warburg coefficient can be estimated from the slope (Z') and the inverse square root of lower angular frequency $\omega^{-\frac{1}{2}}$ $\omega^{-1/2}$ by the relationship[10] as shown in **Figure S3(c)**. The relation between Z' and $\omega^{-1/2}$ is related as per **equation S7**. Accordingly, the Warburg coefficient is directly related to diffusion constant by the **equation S8**[11].

$$Z' = Rs + Rct + \sigma_\omega . \omega^{-1/2} \qquad (S7)$$

$$D = 0.5 \left(\frac{RT}{A\,F^2\,\sigma_W\,C}\right)^2 \qquad (S8)$$

D, R (8.314 J mol^{-1} K^{-1}), F (96500 C mol^{-1}), C (3M KOH), and T (298 K) are the diffusion constant, universal gas constant, the Faraday constant, the electrolyte's molarity, and T is the room temperature. The diffusion coefficient has an important role in the relation between scan rate and peak current in a redox process[12], which can directly contribute as **equation S9**

$$i = n\,F\,A\,C\,D^{\frac{1}{2}}\,\nu^{\frac{1}{2}}\left(\frac{nF}{RT}\right)^{\frac{1}{2}}\pi^{\frac{1}{2}}\,\chi(bt) \qquad (S9)$$

Performing the calculations using **equation S8**, 2×10^{-13} cm^2 s^{-1} value for the K-ion diffusion coefficient for the FeCoNiCrZn liquid state device was obtained, verifying that the K-ion resistance is low, the diffusion path is shortened, and fast charge transfer kinetics is facilitated[13].

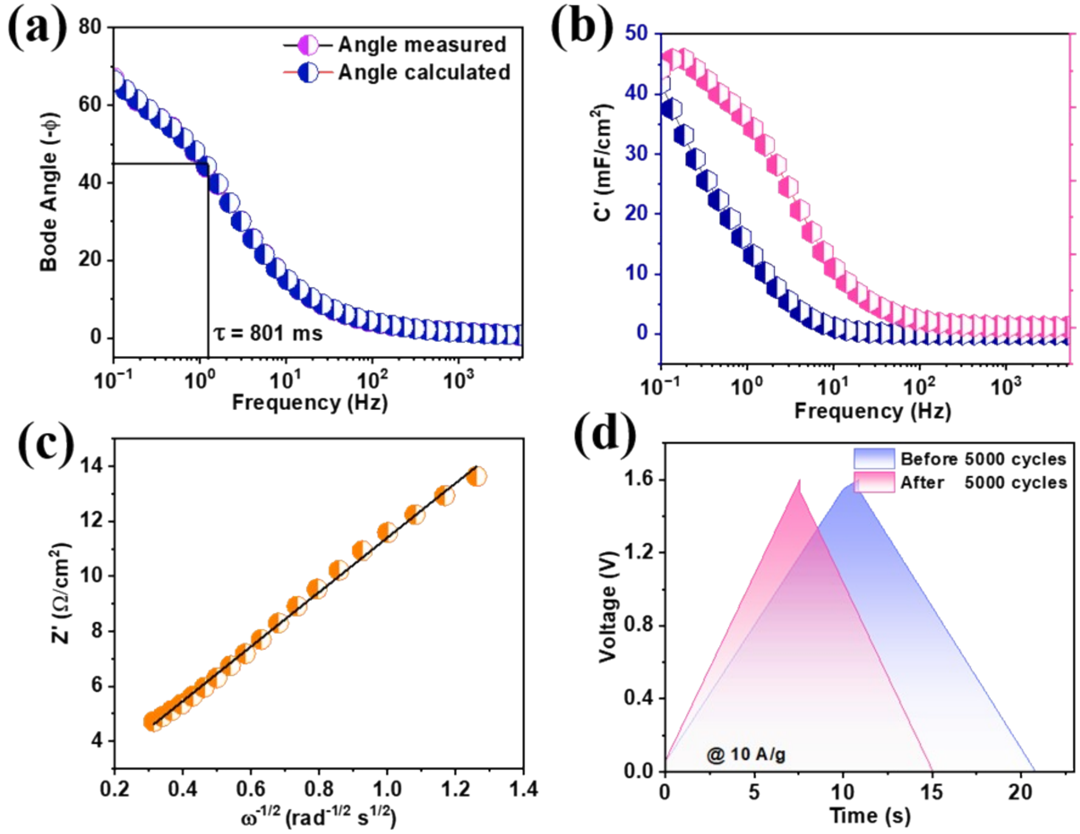

Figure S3: *(a) Bode plot (Phase angle versus frequency) (b) Capacitance component (real and imaginary) versus frequency (c) Warberg plot for evaluation of Warberg coefficient (d) Charge-discharge curve at 10 A* g^{-1} *before and after 5000 cycles.*

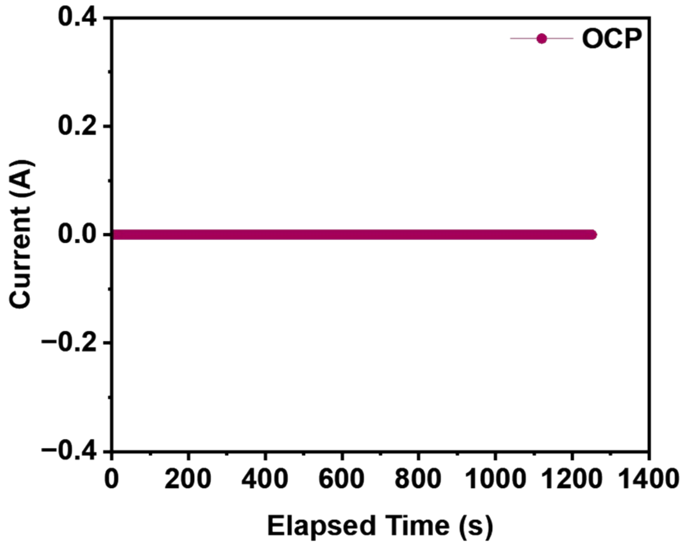

Figure S4: *Open circuit potential of the HEA electrode.*

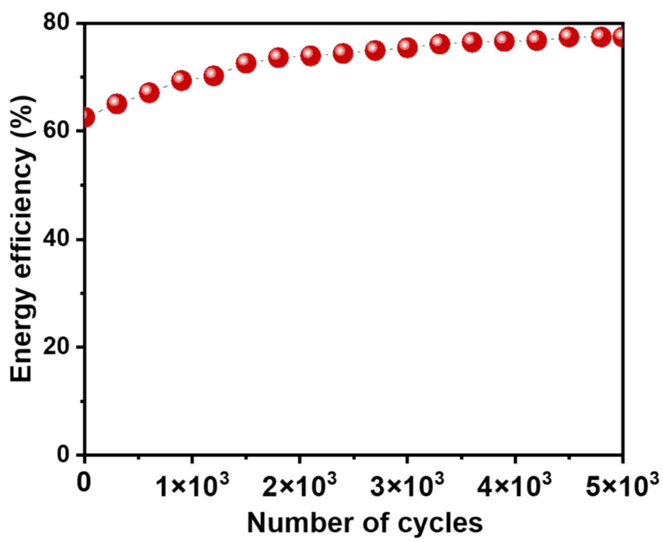

Figure S5: *Energy efficiency plot of the device.*

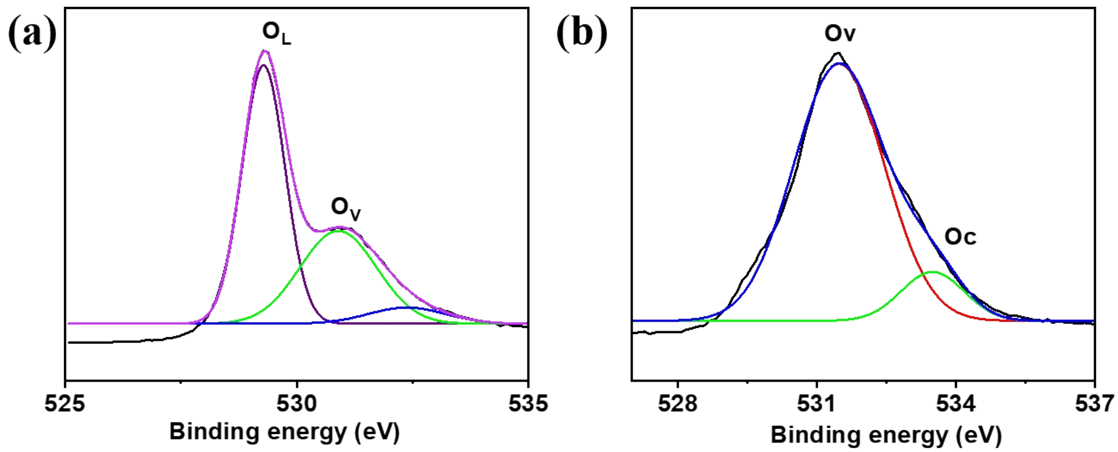

Figure S6: *Oxygen states before and after 5000 cycles.*

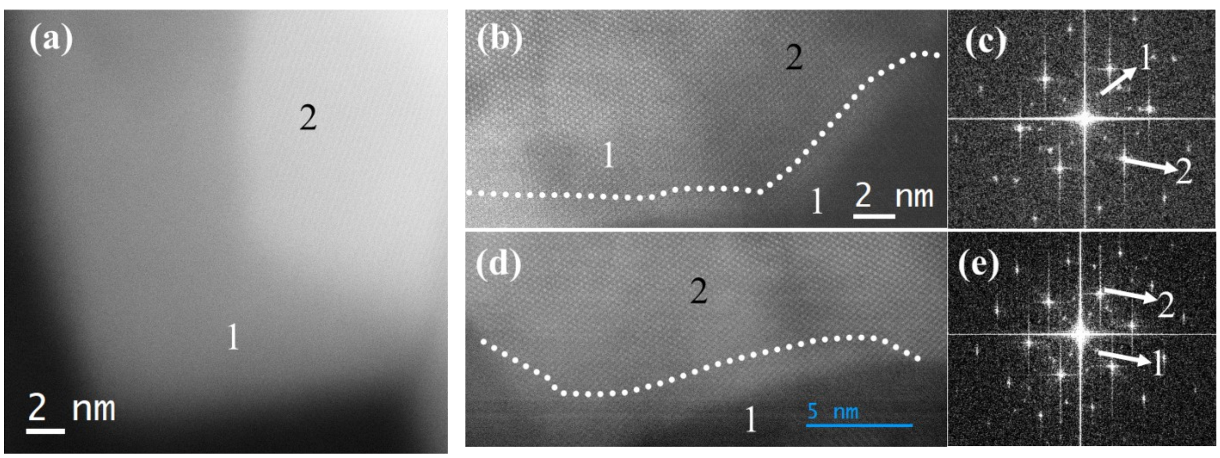

Figure S7: *(a) STEM image in HAADF mode showing bright (2) contrast of HEA and thin oxide layer with light contrast (1) (b) (d) HRSTEM image showing HEA (2) metal with 111 orineted lattice with thin oxide layer (1). The dotted line showing the interface. (c)(e) Diffraction from the particle shows extra spot corresponding to thin oxide layer.*

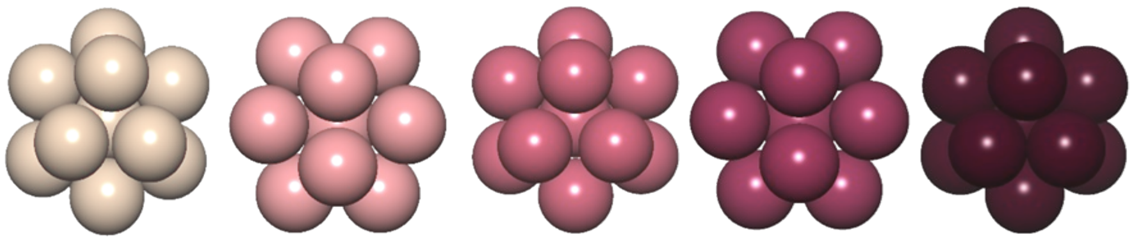

Figure S8: *13-atom icosahedron nanocluster of Cr, Fe, Ni, Co, and Zn (left to right).*

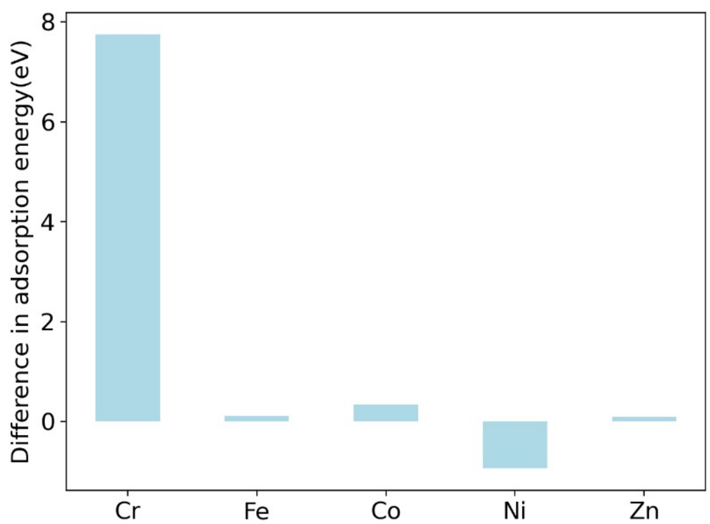

Figure S9: *Difference in adsorption energy of OH on each element of HEA nanocluster and individual element nanocluster.*

References:

(1) Agarwal, A.; Sankapal, B. R. Ultrathin Cu2P2O7 Nanoflakes on Stainless Steel Substrate for Flexible Symmetric All-Solid-State Supercapacitors. *Chem. Eng. J.* **2021**, *422*, 130131. https://doi.org/10.1016/j.cej.2021.130131.

(2) Ensafi, A. A.; Ahmadi, N.; Rezaei, B.; Abdolmaleki, A.; Mahmoudian, M. A New Quaternary Nanohybrid Composite Electrode for a High-Performance Supercapacitor. *Energy* **2018**, *164*, 707–721. https://doi.org/10.1016/j.energy.2018.09.031.

(3) Mai, L.-Q.; Minhas-Khan, A.; Tian, X.; Hercule, K. M.; Zhao, Y.-L.; Lin, X.; Xu, X. Synergistic Interaction between Redox-Active Electrolyte and Binder-Free Functionalized Carbon for Ultrahigh Supercapacitor Performance. *Nat. Commun.* **2013**, *4* (1), 2923.

https://doi.org/10.1038/ncomms3923.

(4) Shao, Y.; El-Kady, M. F.; Sun, J.; Li, Y.; Zhang, Q.; Zhu, M.; Wang, H.; Dunn, B.; Kaner, R. B. Design and Mechanisms of Asymmetric Supercapacitors. *Chem. Rev.* **2018**, *118* (18), 9233–9280. https://doi.org/10.1021/acs.chemrev.8b00252.

(5) Verma, A.; Kim, K. H.; Mathur, S.; Lee, D. Interdependence of the Electrical Performance of NiCuFeCoMn Multi-Structure Carbonates as Electrode Material for Supercapacitors. *J. Alloys Compd.* **2022**, *922*, 166222. https://doi.org/10.1016/j.jallcom.2022.166222.

(6) Lal, M. S.; Sundara, R. High Entropy Oxides—A Cost-Effective Catalyst for the Growth of High Yield Carbon Nanotubes and Their Energy Applications. *ACS Appl. Mater. Interfaces* **2019**, *11* (34), 30846–30857. https://doi.org/10.1021/acsami.9b08794.

(7) Peng, H.; Ma, G.; Sun, K.; Mu, J.; Luo, M.; Lei, Z. High-Performance Aqueous Asymmetric Supercapacitor Based on Carbon Nanofibers Network and Tungsten Trioxide Nanorod Bundles Electrodes. *Electrochim. Acta* **2014**, *147*, 54–61. https://doi.org/10.1016/j.electacta.2014.09.100.

(8) Sahu, V.; Goel, S.; Sharma, R. K.; Singh, G. Zinc Oxide Nanoring Embedded Lacey Graphene Nanoribbons in Symmetric/Asymmetric Electrochemical Capacitive Energy Storage. *Nanoscale* **2015**, *7* (48), 20642–20651. https://doi.org/10.1039/C5NR06083D.

(9) Pandit, B.; Karade, S. S.; Sankapal, B. R. Hexagonal VS 2 Anchored MWCNTs: First Approach to Design Flexible Solid-State Symmetric Supercapacitor Device. *ACS Appl. Mater. Interfaces* **2017**, *9* (51), 44880–44891. https://doi.org/10.1021/acsami.7b13908.

(10) Lalwani, S.; Sahu, V.; Marichi, R. B.; Singh, G.; Sharma, R. K. In Situ Immobilized, Magnetite Nanoplatelets over Holey Graphene Nanoribbons for High Performance Solid State Supercapacitor. *Electrochim. Acta* **2017**, *224*, 517–526. https://doi.org/10.1016/j.electacta.2016.12.057.

(11) Xiao, C.; Zhang, S.; Wang, S.; Xing, Y.; Lin, R.; Wei, X.; Wang, W. ZnO Nanoparticles Encapsulated in a 3D Hierarchical Carbon Framework as Anode for Lithium Ion Battery. *Electrochim. Acta* **2016**, *189*, 245–251. https://doi.org/10.1016/j.electacta.2015.11.045.

(12) Dubal, D. P.; Ayyad, O.; Ruiz, V.; Gómez-Romero, P. Hybrid Energy Storage: The Merging of Battery and Supercapacitor Chemistries. *Chem. Soc. Rev.* **2015**, *44* (7), 1777–1790. https://doi.org/10.1039/C4CS00266K.

(13) Hussain, I.; Lee, J. M.; Iqbal, S.; Kim, H. S.; Jang, S. W.; Jung, J. Y.; An, H. J.; Lamiel, C.; Mohamed, S. G.; Lee, Y. R.; Shim, J.-J. Preserved Crystal Phase and Morphology: Electrochemical Influence of Copper and Iron Co-Doped Cobalt Oxide and Its Supercapacitor Applications. *Electrochim. Acta* **2020**, *340*, 135953. https://doi.org/10.1016/j.electacta.2020.135953.